

Editing 3D Scenes via Text Prompts without Retraining

Shuangkang Fang¹ Yufeng Wang¹ Yi Yang²
Yi-Hsuan Tsai³ Wenrui Ding¹ Shuchang Zhou² Ming-Hsuan Yang^{3,4,5}
¹Beihang University ²Megvii ³Google
⁴University of California, Merced ⁵Yonsei University

arXiv:2309.04917v3 [cs.CV] 30 Nov 2023

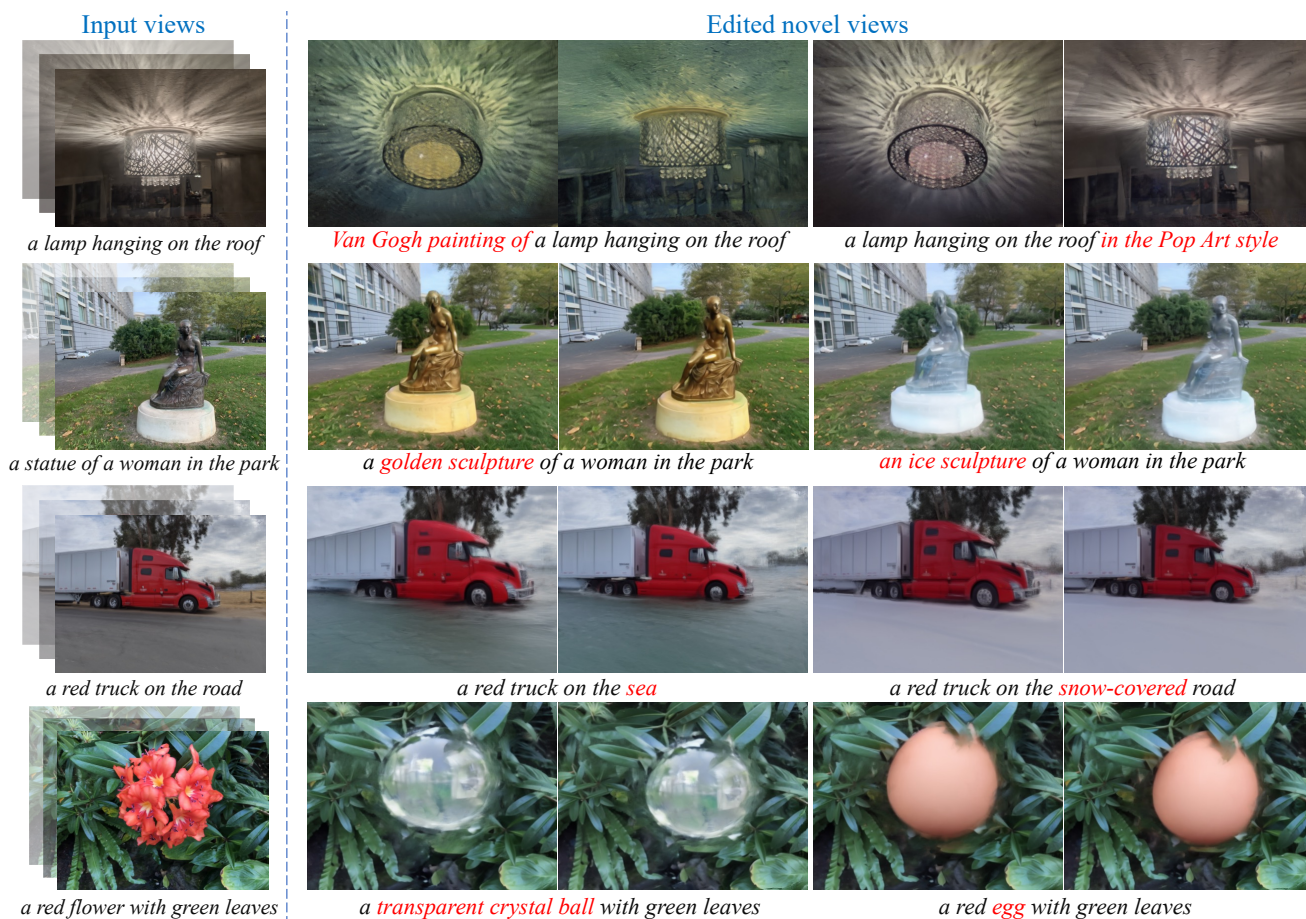


Figure 1. **Visualization results of our method in 3D scene editing.** The proposed DN2N method enables users to obtain realistic and 3D consistent novel views that correspond to the target caption without retraining a new model.

Abstract

Numerous diffusion models have recently been applied to image synthesis and editing. However, editing 3D scenes is still in its early stages. It poses various challenges, such as the requirement to design specific methods for different editing types, retraining new models for various 3D scenes, and

the absence of convenient human interaction during editing. To tackle these issues, we propose a novel text-driven 3D editing method with generalization capability, termed DN2N, which allows for the direct acquisition of the editing results without the requirement for retraining. Our method employs off-the-shelf text-based editing models of 2D images to modify the 3D scene images, followed by a filter-

ing process to discard poorly edited images that disrupt 3D consistency. We then consider the remaining inconsistency as a problem of removing noise perturbations, which can be solved by generating data with similar perturbation characteristics for training. We then propose cross-view regularization terms to help the DN2N model mitigate these perturbations. Empirical results show that our method achieves multiple editing types, including but not limited to appearance editing, weather transition, object changing, and style transfer. Most significantly, our method exhibits strong generalization of editing capabilities, eliminating the need to customize or retrain editing models for specific scenes or editing types. Therefore, it significantly reduces editing time and storage consumption. The project website is available at <https://sk-fun.fun/DN2N>.

1. Introduction

Significant advances in neural radiance fields (NeRF) techniques [1–8] have been modeled for specific types of 3D manipulation, such as appearance editing [9, 10], scene composition [11, 12], weather transformation [13], multiple editing [14, 15], and style transfer [16–20]. Recently, a few attempts have been made to leverage multimodal techniques to design text-guided 3D editing methods [21–23]. Despite the demonstrated success, several challenges remain: (1) many of these techniques [9–20] are less user-friendly; (2) existing methods [9–20] typically rely on known editing types in advance, resulting in limited modification capabilities; (3) retraining an editing model is required [9–23] for each particular 3D scene, leading to computational and memory overhead. To tackle these challenges, in this article, we aim to devise a novel approach that possesses diverse and user-friendly editing capabilities while also having the ability to directly edit new scenes without retraining.

Currently, leveraging existing multimodal models on 2D images [24–27] and NeRF-based framework allows for text-driven 3D scene editing [21–23]. However, these methods are non-generalizable since if we wanted to perform 100 types of editing on 100 scenes, they would require training 10,000 models. In contrast, our research aims to accomplish these edits with a single model. An intuitive solution is to replace the NeRF model in these methods with a generalizable one [6, 28–30]. Nevertheless, directly designing it in this way presents two issues: (1) insufficient task-specific training data to ensure the model’s robust generalization abilities; (2) the inherent 3D inconsistency arising from directly using multimodal 2D image editing models to edit the 3D scenes. To address these issues, we propose directly modeling the inherent 3D inconsistency, and leveraging existing tools to generate sufficient training data with similar characteristics, enabling the model to acquire robust generalization abilities to mitigate this inconsistency.

Specifically, we initially utilize a 2D editing model [27] to perform the preliminary editing on the images of a 3D scene. We subsequently apply a designed content filter to remove several images with poor editing results. The remaining images may still contain inconsistent 3D results, which we consider as minor perturbations to the ideally edited images due to the inherent stochastic and diverse nature of the 2D editing model. To remove such minor perturbations, we generate ample amounts of training data pairs with similar characteristics to train our model: firstly, we utilize the BLIP model [31] and GPT [32] to obtain the input and target captions required for editing, then apply random slight edits to the 3D scene images to simulate the minor perturbations. In this manner, images with added random perturbations are utilized as inputs, while clean images serve as ground truth for training the generalizable model.

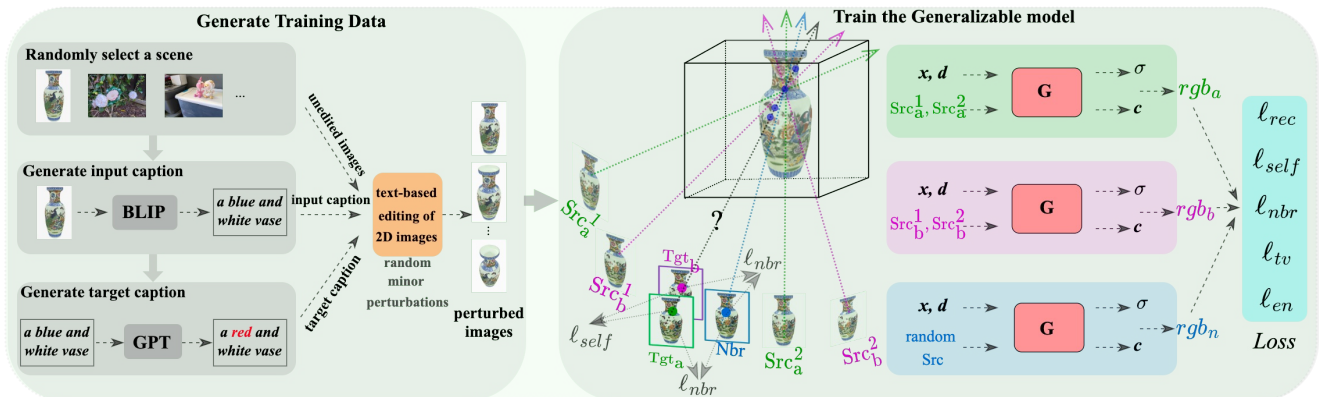
We further introduce two cross-view regularization terms during training to facilitate its 3D consistency, including the self and neighboring views. The former requires the model to generate consistent results for the same target view that is derived from two different source views, while the latter enforces the overlapping pixel values between the target and adjacent views to be approximately close.

The main contributions of this work are:

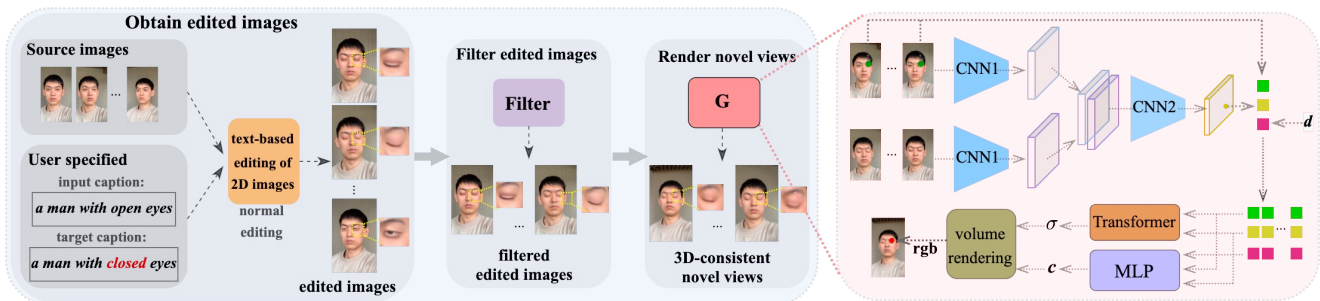
- We develop a 3D scene editing framework with generalization capabilities, named DN2N. It employs off-the-shelf 2D editing models for 3D scene manipulation, where the induced 3D inconsistency is modeled as perturbations and addressed by generating training data pairs with similar perturbation characteristics for optimization.
- We devise a generalizable NeRF model structure. In addition to crafting sufficient training data pairs, we integrate cross-view regularization terms into the model’s training process, enabling it to acquire the capability to eliminate perturbations.
- We conduct extensive experiments of different editing types on multiple datasets. Compared with other approaches, DN2N offers diverse editing capabilities within a shorter time and lower memory overhead, as well as eliminating the necessity for customizing or retraining a model for different scenes or editing types.

2. Related work

NeRF-based novel view synthesis. Novel view synthesis based on NeRF has recently gained significant attention in the vision and graphics communities [1–8]. NeRF represents the structure and appearance of a 3D scene by using a neural network that takes the spatial location and view direction as input and outputs the corresponding color and opacity at each pixel. Subsequent works have improved NeRF, such as speeding up the training process [3, 8], designing better sampling strategies [4], and enhancing generalization ability [6, 28–30].



(a) **Training stage.** *Left:* we generate abundant training data pairs by applying subtle perturbations to all training scenes using the BLIP, GPT, and a 2D editing model. *Right:* we train the generalized NeRF model G by incorporating cross-view regularization terms l_{self} and l_{nbr} . Upon completion of the training process, there is no need to retrain the model for new scenes. Instead, the editing results can be directly obtained through the inference stage.



(b) **Inference stage.** *Left:* we begin by applying standard magnitude editing to the 3D scene images. *Middle:* we devise a content filter to eliminate the images with subpar editing results and compromised consistency. *Right:* then, we utilize the well-trained model G to obtain the edited novel views.

Figure 2. **Illustration of the DN2N framework.** See Sec 3 for the detailed description.

Diffusion-based image editing. Diffusion-based models have been widely used in image generation [33–40]. Numerous text-based image editing methods have recently been developed, such as GLIDE [41] and Stable Diffusion [38]. Imagic [42] finetunes images according to text, and Prompt-to-prompt [25] preserves unedited regions by utilizing cross-attention information. Pix2pix-zero [43] employs embedding vector mechanisms to establish controllable editing directions for images. InstructPix2Pix [26] trains a model by generating a large number of text-editing image pairs using GPT [44] and Stable Diffusion. Null-text inversion [27] proposes an accurate inversion process to enhance image-controlled editing capabilities.

3D scene editing. Numerous 3D scene editing approaches have been developed based on point cloud [45, 46] and triangle meshes representations [47–49]. These methods are limited by their inherent representations, which restrict scalability and editing capability. Recently, NeRF-based methods have been used for 3D scene editing [9–20, 50–52]. However, several aspects of these methods are limited. For instance, they are usually restricted to performing a single editing type. Several methods have overcome this lim-

itation [21–23]. For example, Instruct-N2N [23] enables diverse controllable editing of 3D scenes by pre-editing 2D images using InstructPix2Pix [26]. However, Instruct-N2N also has two notable drawbacks. First, retraining is necessary for each new editing direction, resulting in significant computation and memory overhead. Second, this method requires continuously generating new training data and updating model parameters during training, which is time-consuming and has high storage consumption. In contrast, our method addresses these two challenges by only using a single editing model for all 3D scenes and editing types without the need for retraining, resulting in decreased model storage consumption and training time.

3. Method

Overall framework. The DN2N framework is illustrated in Figure 2. The training stage involves training the model across multiple scenes. For each scene, we first utilize BLIP [31] to obtain its description as the input caption and then employ GPT [32] to randomly modify this caption to create the target caption. We then use a 2D image editing

model [27] to apply minor perturbations to the scene based on these captions to obtain training data pairs. The training objective of our model is to remove these perturbations and reconstruct the 3D scene (see Eq. 4). Besides, we introduce cross-view regularization terms to assist in model training. Specifically, we use two sets of independent source views to render the same target view, resulting in Tgt_a and Tgt_b , respectively, and render a neighboring view around the target view to obtain Nbr . Then we impose a consistency loss (see Eq. 5 and Eq. 6) on the three rendered results. During the inference stage, given a new scene, we begin by applying standard magnitude editing to the scene and filter out images with poor editing effects (see Eq. 9). Finally, we feed the filtered images into the well-trained generalizable model to obtain edited novel views directly.

Optimization objectives. A 3D scene training data consists of N images and their corresponding camera parameters, denoted as $\{I_i, P_i\}_{i=1}^N$. We employ the 2D image editing model \mathcal{F} to obtain the pre-edited image \tilde{I}_i for each I_i , which is defined as:

$$\tilde{I}_i = \mathcal{F}(I_i, C_{in}^i, C_{tgt}^i, \theta), \quad (1)$$

where C_{in}^i is input caption for the unedited image I_i , C_{tgt}^i is target caption for the edited image \tilde{I}_i , and θ is the hyper-parameters of model \mathcal{F} . After filtering out the poorly edited images in $\{\tilde{I}_i, P_i\}_{i=1}^N$, the resulting data is denoted as $\{\tilde{I}_m, P_m\}_{m=1}^M$, where $M \leq N$. Then the generalizable NeRF model G with parameter Θ predicts the target view \hat{I}_m using K source views $\{\tilde{I}_k, P_k\}_{k=1}^K$:

$$\hat{I}_m = G(\tilde{I}_k, P_k, \Theta \mid k = 1, \dots, K, P_k \neq P_m). \quad (2)$$

Assuming that the ideal ground truth (GT) of edited images with 3D consistency is denoted as I_m^{gt} , our optimization objective can be expressed as:

$$\arg \min_{\Theta} \sum_{m=1}^M \left\| I_m^{gt} - \hat{I}_m \right\|^2. \quad (3)$$

However, the GT is not at our disposal. Thus, we express the pre-edited image \tilde{I}_m as $\tilde{I}_m = I_m^{gt} + \Delta I_m$. This implies that the inconsistent image \tilde{I}_m can be perceived as consistent GT image I_m^{gt} with minor perturbations ΔI_m . If our model G can learn the ability to remove ΔI_m from the \tilde{I}_m , then we can obtain the consistent editing results since $I_m^{gt} = \tilde{I}_m - \Delta I_m$. In this work, the perturbations ΔI_m mainly stem from the inherent editing characteristics of model \mathcal{F} . Hence, we apply similar random minor perturbations ΔI_i to clean 3D scene images $\{I_i\}_{i=1}^N$ by controlling the parameters θ in \mathcal{F} to get the training data $\{\tilde{I}_i, P_i\}_{i=1}^N$. Then, the unedited images $\{I_i\}_{i=1}^N$ can be used as pseudo ground truth

to train the model G as follows:

$$\arg \min_{\Theta} \sum_{i=1}^N \left\| I_i - G(\tilde{I}_k, P_k, \Theta \mid k = 1, \dots, K, P_k \neq P_i) \right\|^2. \quad (4)$$

Generate training data. To generate training data pairs, we utilize the off-the-shelf tools BLIP [31] and GPT [32]. As illustrated in Figure 2, we randomly select a scene and feed its one image into the BLIP to obtain its input caption, such as “a blue and white vase.” Subsequently, we use GPT to rewrite the input caption to generate the target caption, such as “a red and white vase.” For each image of a scene, we apply randomly minor perturbations by controlling the hyper-parameters θ in Eq. 1. For detailed parameter settings, please refer to the supplementary materials.

Self-view robustness loss. We use a training approach similar to that in the generalizable NeRF models [6, 29, 30], which involves predicting the target view based on several source views. Unlike these methods, our training data incorporates minor perturbations. In addition to reconstructing 3D scenes, our model’s training objective also aims to remove these perturbations that cause inconsistencies. To achieve this, we perform two independent predictions, labeled \mathcal{A} and \mathcal{B} . For \mathcal{A} , we use source views $\{Src_a^1, Src_a^2, \dots\}$ to predict the target view Tgt_a . Additionally, for \mathcal{B} , we use different source views $\{Src_b^1, Src_b^2, \dots\}$ to predict the same target view Tgt_b . Then, we calculate the L2 loss to ensure consistency between the two predictions:

$$\ell_{self} = \|Tgt_a - Tgt_b\|^2. \quad (5)$$

Neighboring view consistency loss. Empirically, we observe that there are often noticeable texture or color discontinuities between adjacent views when rendering along a smooth camera path. To tackle this issue, we enforce a smooth transition between adjacent views. Specifically, we slightly perturb the pose corresponding to the target view and generate a neighboring view Tgt_{nbr} based on the perturbed pose. We then project the pixel points from the target view onto the neighboring view using the depth rendered by model G . We further minimize the following loss to reduce image discontinuities caused by changes in the viewing angle:

$$\ell_{nbr} = \|M(Tgt_a - Tgt_{nbr})\|^2 + \|M(Tgt_b - Tgt_{nbr})\|^2, \quad (6)$$

where M refers to a mask that discards some pixels on the target view that are not visible to the neighboring view.

In addition, we note that the weights of some sampled points are uniformly distributed along the rays, leading to floating objects in the predicted results and inaccurate depth estimates, which may affect the accuracy of the target view to neighboring view projection. Thus, we introduce an entropy loss [53] for the weights of the sampled points:

$$\ell_{en} = -\sum T_i(1 - \exp(-\sigma_i\delta_i)) \log(T_i(1 - \exp(-\sigma_i\delta_i))), \quad (7)$$

where $T_i = \exp(-\sum_{j=1}^{i-1} \sigma_j\delta_j)$. σ_i is the density of the sampled points and δ_i denotes the distance between adjacent sampled points.

Total loss. During training, the model cannot render a complete image in a single forward pass due to GPU memory limitations. Thus, the loss is computed on a patch level, and the total loss function employed in this work is:

$$\ell = \ell_{rec} + \lambda_1\ell_{self} + \lambda_2\ell_{nbr} + \lambda_3\ell_{en} + \lambda_4\ell_{tv}, \quad (8)$$

where ℓ_{rec} is the reconstruction loss obtained from Eq. 4, and ℓ_{tv} is the total variation regularization term [54].

Content filter. During the inference stage, applying normal amplitude edits to 3D scene images may produce extremely poor editing results for certain views. These poor editing results cannot be fully remedied solely through the model G . Therefore, we designed a content filter first to remove these images. After this step, only minor perturbations remain, which can be eliminated using the well-trained model G . Combining evaluations of editing results from previous methods [22, 23], we propose a content filter based on the following four tuples:

- 1.SSIM(I_i, \tilde{I}_i), 2.CLIP(\tilde{I}_i, C_{tgt}), 3.CLIP(I_i, \tilde{I}_i),
- 4.CLIP(I_i, \tilde{I}_i) - CLIP(C_{in}, C_{tgt}).

For all edited images, we compute the above four metrics and sort them individually. Then, we discard the top and bottom 10% of outlier images for each metric, retaining only values close to the mean to reduce the differences among the edited images. In our experiments, approximately 30% of the images are ultimately filtered out. In cases where the discarded images exceed 50%, we will employ the model G to generate new images to mitigate data scarcity. Filtered examples and numerical results for each metric can be found in the supplementary materials.

Network structure. The generalizable NeRF model G in Figure 2 is developed based on the IBRNet [6]. We extend it by incorporating multi-viewpoint aggregation, cross-view mappings, and integration of unedited image information to render consistent results. More details regarding the model G are described in the supplementary materials.

4. Experiments and Analysis

The scenes used to train our model are from Google Scanned Objects [55], NeRF-Synthetic [1], Spaces [56] and the IBRNet-collect [6]. The LLFF [57] and NeRF-Art [22] datasets are used for evaluation. Also, all text prompts displayed in the experimental results are not used for training.

Furthermore, we also verify DN2N on the OMMO [58] in the UAV’s 360-degree view and the KITTI [59] in the vehicle’s view (The experimental results of these two data are shown in supplementary materials). The default 2D-image editing model is Null-text [27]. We implement our method with PyTorch [60], train the model on 8 NVIDIA V100 GPUs, and use one single V100 GPU for inference. For more implementation details, experimental results, and video demos, please see the supplementary materials.

4.1. Qualitative results

As illustrated in Figure 1, our approach demonstrates its ability to achieve various challenging editing types without retraining while maintaining 3D consistency and conforming to the text description. To further assess the effectiveness of our approach, we conduct comparative studies against state-of-the-art methods.

Text-driven 3D scene editing. We compare our approach to other text-driven editing methods in Figure 3. NeRF-Art utilizes multiple loss functions to retrain a model when given target words, with limitations in achieving complex and precise editing effects. Instruct-N2N initially edits 2D images according to instruction and trains a model using these images, then generates new images to train the model recurrently until it produces images that comply with the instructions, which consumes a substantial amount of computational and storage resources. In contrast, the scene editing results by DN2N are directly inferred after giving a text without any intervening training process. In addition, the editing results by DN2N are more realistic and retain more areas unrelated to the target caption, as shown in Figure 3.

Appearance editing. Two implicit steps are involved in editing the appearance of an object in a scene: determining the target area and editing the appearance of that area. As illustrated in Figure 4, our method accurately locates the target area and applies appearance editing consistent with the target description without requiring training. While Clip-NeRF uses CLIP Similarity to limit the novel view to the target words, it cannot accurately locate the target area. DFF uses DINO or Lseg to inject label information into points in space, ensuring precise editing area localization. However, its appearance editing requires manual operations, such as specifying the RGB value of the editing area. Furthermore, both methods require training separate models for each scene, making them less efficient than DN2N.

Style transfer. Figure 5 presents visual comparisons rendered by DN2N and other 3D scene style transfer techniques. As depicted, the Learning-to-Stylize method tends to imitate the color information of the reference image, but it often overlooks curved strokes. On the other hand, ARF excessively imitates curved strokes of the reference image, resulting in less pleasing visual effects and loss of information in the original scene. In contrast, our approach synthe-

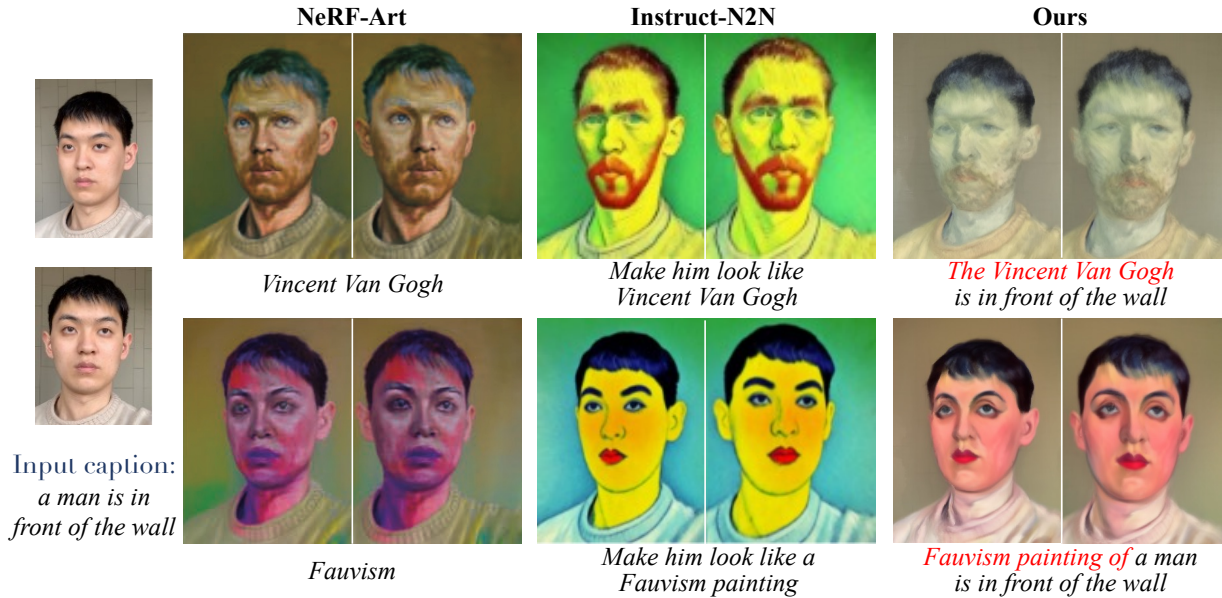


Figure 3. **Comparison with other text-driven editing methods.** DN2N strikes a better balance between preserving image content and aligning with textual descriptions. More importantly, it is not necessary to retrain our model for different editing types.

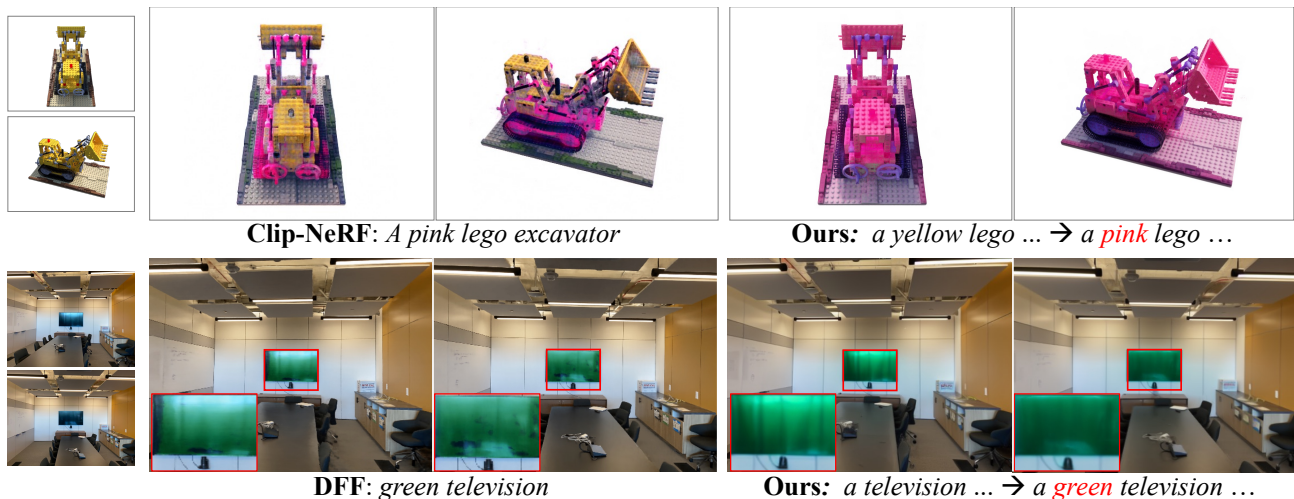


Figure 4. **Comparison with other methods for editing appearance.** DN2N achieves higher accuracy in matching target captions while effectively preserving information in non-edited areas.

sizes the scenes by capturing both the color and stroke of the target style. Furthermore, both Learning-to-Style and ARF necessitate selecting a reference image first and then training an editing model, making them less efficient and practical than the DN2N method.

4.2. Quantitative results

Ability to resist perturbations. Our method is specifically designed for scene editing, capable of maintaining 3D consistency under minor editing perturbations. To demonstrate this, we compare our approach to commonly used general-

ization models in 8 scenes on the LLFF dataset. Table 1 shows the results of two types of comparisons: one on unedited scenes (LLFF) and the other on scenes with minor editing perturbations (LLFF*). It can be seen that our approach outperforms other models on scenes with minor perturbations resulting from 2D editing. Figure 6 also illustrates that our method can achieve superior 3D consistency in editing outcomes, which demonstrates our method is more suitable for the 3D scene editing task.

Model efficiency. Our generalizable model precludes re-training, which is more efficient and practical. A compari-



Figure 5. **Comparison with other methods for editing scene styles.** DN2N can more accurately transfer colors and brush strokes while preserving more original image content.

Table 1. **Comparison of mean PSNR with other generalizable NeRF models on the LLFF dataset.** * indicates random minor perturbations to the scenes.

	LLFF	LLFF*
PixelNeRF	18.66	11.03
MVSNerF	21.18	16.74
IBRNet	25.17	20.05
Neuray	25.35	19.31
DN2N	23.81	22.42

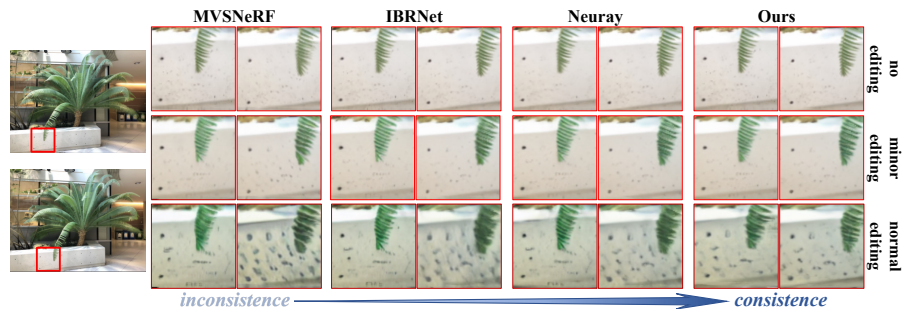


Figure 6. **Comparison with other generalizable NeRF models on the fern scene.** Our approach can maintain 3D consistency across novel views under different editing degrees.

Table 2. **Quantitative comparison of time and model size for editing the flower scene in LLFF dataset.** ‘TC’ and ‘SC’ stand for Time and Space Complexity, respectively.

	time (minute)			TC	Size(MB)	SC
	train	edit	total			
ARF	21.7	3.4	25.1	$O(n)$	558	$O(n)$
DFF	20.6	5.2	25.8	$O(n)$	144	$O(n)$
Clip-NeRF	524.4	349.7	874.1	$O(n)$	29.4	$O(n)$
NeRF-Art	1545.6	780.6	2326.2	$O(n)$	18.3	$O(n)$
Instruct-N2N	19.2	62.1	81.3	$O(n)$	484	$O(n)$
Ours	0	22.3	22.3	$O(n)$	103	$O(1)$

son of model efficiency has been incorporated, and the results, as depicted in Table 2, show substantial advantages of the proposed DN2N over state-of-the-art techniques in running time and model storage. In terms of running time, our approach does not require training for new scenes or new types of edits, only necessitating inference time for editing, resulting in being more time-efficient than alternative

techniques. Regarding model storage, our model, which is applicable across all scenes and types of edits, entails a constant space complexity of $O(1)$, while other methods necessitate space complexity of $O(n)$. When users intend to perform 100 different types of edits on 100 scenes, comparative methods necessitate the training and storage of 10,000 new models, whereas our method requires only one model.

4.3. User study

We perform a user study to further analyze the editing results of the proposed method against state-of-the-art approaches. We invited 50 participants to make a preference choice in editing results between DN2N and other methods, yielding 1700 votes in total for three evaluation metrics: 3D consistency, preservation of the original scene content, and faithfulness to the text description. The results are depicted in Figure 7, which shows that DN2N is favored in terms of these evaluation metrics. The implementation details of the user study can be found in the supplementary materials.

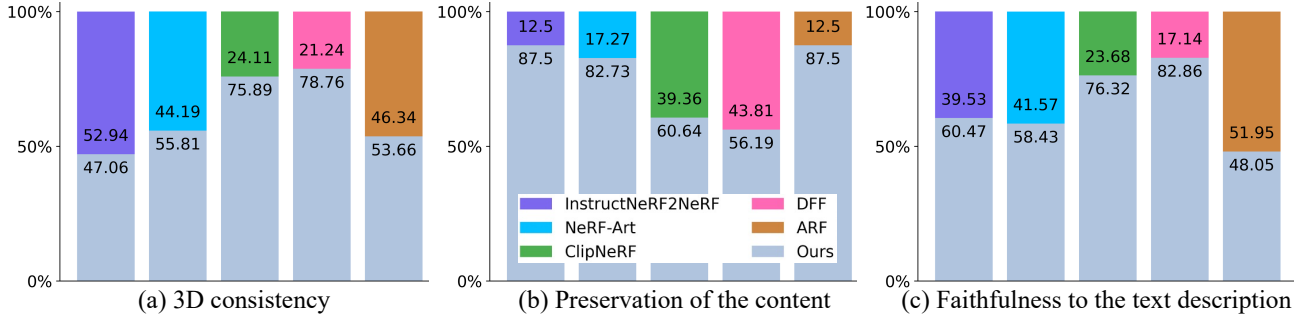


Figure 7. **User study.** The proposed DN2N method performs well against other state-of-the-art approaches in terms of comprehensive performance across three evaluation criteria.

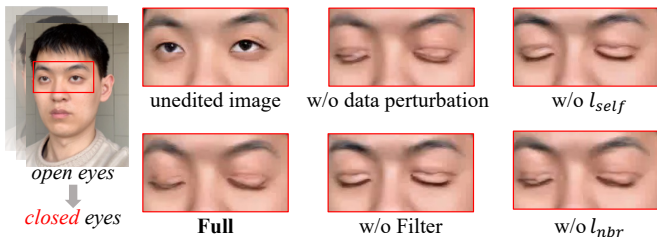


Figure 8. **Ablation studies for key components in DN2N.** We recommend referring to the *video demo* in the supplementary materials to observe the consistency differences.



Figure 9. **Failed editing cases.** The editing result is limited by the 2D multimodal model.

Table 3. **PSNR results of ablation studies.** Experiments are conducted by applying four random minor perturbations to the scene editing in Figure 8. DP denotes data perturbation.

	w/o DP	w/o l_{self}	w/o l_{nbr}	Full
exp1	17.24	19.89	21.05	21.76
exp2	18.98	21.5	21.92	23.11
exp3	18.73	21.16	22.39	24.21
exp4	18.97	20.53	22.19	22.27

4.4. Ablation studies

We demonstrate the contribution of each component in our method in Figure 8. We find that the absence content filter results in significant image distortion. This can be attributed to the fact that applying normal amplitude edits to 3D scene images may produce extremely poor editing results for a few views, making it difficult for the model to solve these inconsistencies without the content filter. Omitting the data perturbation process or removing the cross-view regularization terms during training would significantly affect the model performance on edited results. Furthermore, we directly evaluate DN2N’s ability to remove perturbations by applying several random disturbances to the scene depicted in Figure 8. The PSNR results are presented in Table 3. It is clear that training the generalization model with perturbed data is crucial and enforcing cross-view consistency

can also enhance the model’s overall performance.

4.5. Limitations

When utilizing 2D multimodal models for 3D scene editing, a common limitation arises wherein the 3D editing outcomes heavily depend on 2D methods, making it challenging to achieve editing beyond the capabilities of the 2D model. For instance, CLIP-NeRF [21] is limited by the CLIP model [24], while Instruct-N2N [23] is influenced by the results of InstructPix2Pix [26]. Similarly, our approach is also constrained by Null-text [27]. As shown in Figure 9, 2D editing models may not always achieve reliable editing results, leading to failures in editing 3D scenes.

5. Conclusion

In this work, we propose a text-driven method for editing 3D scenes that exhibits strong generalization capabilities and enables realistic novel view editing without additional training for each modification task. Our approach leverages existing 2D editing models to perform initial editing of 3D scene data based on textual prompts. We then filter out poorly edited images, treating the remaining inconsistency as perturbations on top of consistently edited results. To eliminate this perturbation, we provide several approaches to train our model, including creating training data and strengthening cross-view robustness. The experimental re-

sults demonstrate the effectiveness of our approach, which offers significant advantages over other methods. Specifically, our method provides greater convenience for editing, supports multiple editing capabilities, and eliminates the need for training on new scenes, thus significantly reducing the editing time and model storage requirements.

References

- [1] Ben Mildenhall, Pratul P Srinivasan, Matthew Tancik, Jonathan T Barron, Ravi Ramamoorthi, and Ren Ng. Nerf: Representing scenes as neural radiance fields for view synthesis. In *ECCV*, pages 405–421, 2020. 2, 5, 8
- [2] Alex Yu, Ruilong Li, Matthew Tancik, Hao Li, Ren Ng, and Angjoo Kanazawa. Plenotrees for real-time rendering of neural radiance fields. In *ICCV*, pages 5752–5761, 2021.
- [3] Thomas Müller, Alex Evans, Christoph Schied, and Alexander Keller. Instant neural graphics primitives with a multi-resolution hash encoding. *arXiv preprint arXiv:2201.05989*, 2022. 2
- [4] Jonathan T Barron, Ben Mildenhall, Matthew Tancik, Peter Hedman, Ricardo Martin-Brualla, and Pratul P Srinivasan. Mip-nerf: A multiscale representation for anti-aliasing neural radiance fields. In *ICCV*, pages 5855–5864, 2021. 2
- [5] Kai Zhang, Gernot Riegler, Noah Snavely, and Vladlen Koltun. Nerf++: Analyzing and improving neural radiance fields. *arXiv preprint arXiv:2010.07492*, 2020.
- [6] Qianqian Wang, Zhicheng Wang, Kyle Genova, Pratul P Srinivasan, Howard Zhou, Jonathan T Barron, Ricardo Martin-Brualla, Noah Snavely, and Thomas Funkhouser. Ibrnet: Learning multi-view image-based rendering. In *CVPR*, pages 4690–4699, 2021. 2, 4, 5, 1
- [7] Chen-Hsuan Lin, Wei-Chiu Ma, Antonio Torralba, and Simon Lucey. Barf: Bundle-adjusting neural radiance fields. In *ICCV*, pages 5741–5751, 2021.
- [8] Anpei Chen, Zexiang Xu, Andreas Geiger, Jingyi Yu, and Hao Su. Tensorf: Tensorial radiance fields. *arXiv preprint arXiv:2203.09517*, 2022. 2
- [9] Ricardo Martin-Brualla, Noha Radwan, Mehdi SM Sajjadi, Jonathan T Barron, Alexey Dosovitskiy, and Daniel Duckworth. Nerf in the wild: Neural radiance fields for unconstrained photo collections. In *CVPR*, pages 7210–7219, 2021. 2, 3
- [10] Sosuke Kobayashi, Eiichi Matsumoto, and Vincent Sitzmann. Decomposing nerf for editing via feature field distillation. *arXiv preprint arXiv:2205.15585*, 2022. 2
- [11] Jiaxiang Tang, Xiaokang Chen, Jingbo Wang, and Gang Zeng. Compressible-composable nerf via rank-residual decomposition. *arXiv preprint arXiv:2205.14870*, 2022. 2
- [12] Matthew Tancik, Vincent Casser, Xinchun Yan, Sabeek Pradhan, Ben Mildenhall, Pratul P Srinivasan, Jonathan T Barron, and Henrik Kretzschmar. Block-nerf: Scalable large scene neural view synthesis. In *CVPR*, pages 8248–8258, 2022. 2
- [13] Yuan Li, Zhi-Hao Lin, David Forsyth, Jia-Bin Huang, and Shenlong Wang. Climatenerf: Physically-based neural rendering for extreme climate synthesis. *arXiv preprint arXiv:2211.13226*, 2022. 2
- [14] Shuangkang Fang, Weixin Xu, Heng Wang, Yi Yang, Yufeng Wang, and Shuchang Zhou. One is all: Bridging the gap between neural radiance fields architectures with progressive volume distillation. *arXiv preprint arXiv:2211.15977*, 2022. 2
- [15] Shuangkang Fang, Yufeng Wang, Yi Yang, Weixin Xu, Heng Wang, Wenrui Ding, and Shuchang Zhou. Pvd-al: Progressive volume distillation with active learning for efficient conversion between different nerf architectures. *arXiv preprint arXiv:2304.04012*, 2023. 2
- [16] Yi-Hua Huang, Yue He, Yu-Jie Yuan, Yu-Kun Lai, and Lin Gao. Stylizednerf: consistent 3d scene stylization as stylized nerf via 2d-3d mutual learning. In *CVPR*, pages 18342–18352, 2022. 2
- [17] Jiatao Gu, Lingjie Liu, Peng Wang, and Christian Theobalt. Stylenerf: A style-based 3d aware generator for high-resolution image synthesis. In *ICLR*, pages 1–25, 2022.
- [18] Thu Nguyen-Phuoc, Feng Liu, and Lei Xiao. Snerf: stylized neural implicit representations for 3d scenes. *arXiv preprint arXiv:2207.02363*, 2022.
- [19] Zhiwen Fan, Yifan Jiang, Peihao Wang, Xinyu Gong, Dejia Xu, and Zhangyang Wang. Unified implicit neural stylization. In *ECCV*, pages 636–654, 2022.
- [20] Kai Zhang, Nick Kolkin, Sai Bi, Fajun Luan, Zexiang Xu, Eli Shechtman, and Noah Snavely. Arf: Artistic radiance fields. In *ECCV*, pages 717–733, 2022. 2, 3
- [21] Can Wang, Menglei Chai, Mingming He, Dongdong Chen, and Jing Liao. Clip-nerf: Text-and-image driven manipulation of neural radiance fields. In *CVPR*, pages 3835–3844, 2022. 2, 3, 8
- [22] Can Wang, Ruixiang Jiang, Menglei Chai, Mingming He, Dongdong Chen, and Jing Liao. Nerf-art: Text-driven neural radiance fields stylization. *arXiv preprint arXiv:2212.08070*, 2022. 5
- [23] Ayaan Haque, Matthew Tancik, Alexei A Efros, Aleksander Holynski, and Angjoo Kanazawa. Instruct-nerf2nerf: Editing 3d scenes with instructions. *arXiv preprint arXiv:2303.12789*, 2023. 2, 3, 5, 8, 4
- [24] Alec Radford, Jong Wook Kim, Chris Hallacy, Aditya Ramesh, Gabriel Goh, Sandhini Agarwal, Girish Sastry, Amanda Askell, Pamela Mishkin, Jack Clark, et al. Learning transferable visual models from natural language supervision. In *ICML*, pages 8748–8763, 2021. 2, 8
- [25] Amir Hertz, Ron Mokady, Jay Tenenbaum, Kfir Aberman, Yael Pritch, and Daniel Cohen-Or. Prompt-to-prompt image editing with cross attention control. *arXiv preprint arXiv:2208.01626*, 2022. 3
- [26] Tim Brooks, Aleksander Holynski, and Alexei A Efros. Instructpix2pix: Learning to follow image editing instructions. *arXiv preprint arXiv:2211.09800*, 2022. 3, 8
- [27] Ron Mokady, Amir Hertz, Kfir Aberman, Yael Pritch, and Daniel Cohen-Or. Null-text inversion for editing real images using guided diffusion models. *arXiv preprint arXiv:2211.09794*, 2022. 2, 3, 4, 5, 8
- [28] Anpei Chen, Zexiang Xu, Fuqiang Zhao, Xiaoshuai Zhang, Fanbo Xiang, Jingyi Yu, and Hao Su. Mvsnerf: Fast generalizable radiance field reconstruction from multi-view stereo. In *ICCV*, pages 14124–14133, 2021. 2

- [29] Yuan Liu, Sida Peng, Lingjie Liu, Qianqian Wang, Peng Wang, Christian Theobalt, Xiaowei Zhou, and Wenping Wang. Neural rays for occlusion-aware image-based rendering. In *CVPR*, pages 7824–7833, 2022. 4
- [30] Mohammad Mahdi Johari, Yann Lepoittevin, and François Fleuret. Geonerf: Generalizing nerf with geometry priors. In *CVPR*, pages 18365–18375, 2022. 2, 4
- [31] Junnan Li, Dongxu Li, Silvio Savarese, and Steven Hoi. Blip-2: Bootstrapping language-image pre-training with frozen image encoders and large language models. *arXiv preprint arXiv:2301.12597*, 2023. 2, 3, 4, 1
- [32] Tom Brown, Benjamin Mann, Nick Ryder, Melanie Subbiah, Jared D Kaplan, Prafulla Dhariwal, Arvind Neelakantan, Pranav Shyam, Girish Sastry, Amanda Askell, et al. Language models are few-shot learners. In *NeurIPS*, pages 1877–1901, 2020. 2, 3, 4, 1
- [33] Jascha Sohl-Dickstein, Eric Weiss, Niru Maheswaranathan, and Surya Ganguli. Deep unsupervised learning using nonequilibrium thermodynamics. In *ICML*, pages 2256–2265, 2015. 3
- [34] Prafulla Dhariwal and Alexander Nichol. Diffusion models beat gans on image synthesis. In *NeurIPS*, pages 8780–8794, 2021.
- [35] Jonathan Ho, Ajay Jain, and Pieter Abbeel. Denoising diffusion probabilistic models. In *NeurIPS*, pages 6840–6851, 2020.
- [36] Chitwan Saharia, William Chan, Saurabh Saxena, Lala Li, Jay Whang, Emily L Denton, Kamyar Ghasemipour, Raphael Gontijo Lopes, Burcu Karagol Ayan, Tim Salimans, et al. Photorealistic text-to-image diffusion models with deep language understanding. In *NeurIPS*, pages 36479–36494, 2022.
- [37] Aditya Ramesh, Prafulla Dhariwal, Alex Nichol, Casey Chu, and Mark Chen. Hierarchical text-conditional image generation with clip latents. *arXiv preprint arXiv:2204.06125*, 2022.
- [38] Robin Rombach, Andreas Blattmann, Dominik Lorenz, Patrick Esser, and Björn Ommer. High-resolution image synthesis with latent diffusion models. In *CVPR*, pages 10684–10695, 2022. 3
- [39] Jiaming Song, Chenlin Meng, and Stefano Ermon. Denoising diffusion implicit models. In *ICLR*, 2021. 1
- [40] Yang Song, Jascha Sohl-Dickstein, Diederik P Kingma, Abhishek Kumar, Stefano Ermon, and Ben Poole. Score-based generative modeling through stochastic differential equations. In *ICLR*, 2021. 3
- [41] Alexander Quinn Nichol, Prafulla Dhariwal, Aditya Ramesh, Pranav Shyam, Pamela Mishkin, Bob McGrew, Ilya Sutskever, and Mark Chen. Glide: Towards photorealistic image generation and editing with text-guided diffusion models. In *ICML*, pages 16784–16804, 2022. 3
- [42] Bahjat Kawar, Shiran Zada, Oran Lang, Omer Tov, Huiwen Chang, Tali Dekel, Inbar Mosseri, and Michal Irani. Imagic: Text-based real image editing with diffusion models. *arXiv preprint arXiv:2210.09276*, 2022. 3
- [43] Gaurav Parmar, Krishna Kumar Singh, Richard Zhang, Yijun Li, Jingwan Lu, and Jun-Yan Zhu. Zero-shot image-to-image translation. *arXiv preprint arXiv:2302.03027*, 2023. 3
- [44] Tom Brown, Benjamin Mann, Nick Ryder, Melanie Subbiah, Jared D Kaplan, Prafulla Dhariwal, Arvind Neelakantan, Pranav Shyam, Girish Sastry, Amanda Askell, et al. Language models are few-shot learners. In *NeurIPS*, pages 1877–1901, 2020. 3
- [45] Hsin-Ping Huang, Hung-Yu Tseng, Saurabh Saini, Maneesh Singh, and Ming-Hsuan Yang. Learning to stylize novel views. In *ICCV*, pages 13869–13878, 2021. 3
- [46] Fangzhou Mu, Jian Wang, Yicheng Wu, and Yin Li. 3d photo stylization: Learning to generate stylized novel views from a single image. In *CVPR*, pages 16273–16282, 2022. 3
- [47] Qian-Yi Zhou and Vladlen Koltun. Color map optimization for 3d reconstruction with consumer depth cameras. *ACM TOG*, 33(4):1–10, 2014. 3
- [48] Lukas Höllein, Justin Johnson, and Matthias Nießner. Stylemesh: Style transfer for indoor 3d scene reconstructions. In *CVPR*, pages 6198–6208, 2022.
- [49] Fangzhou Han, Shuquan Ye, Mingming He, Menglei Chai, and Jing Liao. Exemplar-based 3d portrait stylization. *IEEE TVCG*, 29(2):1371–1383, 2021. 3
- [50] Mark Boss, Raphael Braun, Varun Jampani, Jonathan T Barron, Ce Liu, and Hendrik Lensch. Nerf: Neural reflectance decomposition from image collections. In *ICCV*, pages 12684–12694, 2021. 3
- [51] Mark Boss, Varun Jampani, Raphael Braun, Ce Liu, Jonathan Barron, and Hendrik Lensch. Neural-pil: Neural pre-integrated lighting for reflectance decomposition. In *NeurIPS*, pages 10691–10704, 2021.
- [52] Fangzhou Mu, Jian Wang, Yicheng Wu, and Yin Li. 3d photo stylization: Learning to generate stylized novel views from a single image. In *CVPR*, pages 16273–16282, 2022. 3
- [53] Mijeong Kim, Seonguk Seo, and Bohyung Han. Infonerf: Ray entropy minimization for few-shot neural volume rendering. In *CVPR*, pages 12912–12921, 2022. 4
- [54] Leonid I Rudin and Stanley Osher. Total variation based image restoration with free local constraints. In *ICIP*, pages 31–35, 1994. 5
- [55] Laura Downs, Anthony Francis, Nate Koenig, Brandon Kinman, Ryan Hickman, Krista Reymann, Thomas B McHugh, and Vincent Vanhoucke. Google scanned objects: A high-quality dataset of 3d scanned household items. In *ICRA*, pages 2553–2560, 2022. 5
- [56] John Flynn, Michael Broxton, Paul Debevec, Matthew DuVall, Graham Fyffe, Ryan Overbeck, Noah Snavely, and Richard Tucker. Deepview: View synthesis with learned gradient descent. In *CVPR*, pages 2367–2376, 2019. 5
- [57] Ben Mildenhall, Pratul P Srinivasan, Rodrigo Ortiz-Cayon, Nima Khademi Kalantari, Ravi Ramamoorthi, Ren Ng, and Abhishek Kar. Local light field fusion: Practical view synthesis with prescriptive sampling guidelines. *ACM TOG*, 38(4):1–14, 2019. 5
- [58] Chongshan Lu, Fukun Yin, Xin Chen, Tao Chen, Gang Yu, and Jiayuan Fan. A large-scale outdoor multi-modal dataset and benchmark for novel view synthesis and implicit scene reconstruction. *arXiv preprint arXiv:2301.06782*, 2023. 5, 8
- [59] Andreas Geiger, Philip Lenz, Christoph Stiller, and Raquel Urtasun. Vision meets robotics: The kitti dataset. *IJRR*, 32(11):1231–1237, 2013. 5, 8

- [60] Adam Paszke, Sam Gross, Francisco Massa, Adam Lerer, James Bradbury, Gregory Chanan, Trevor Killeen, Zeming Lin, Natalia Gimelshein, Luca Antiga, et al. Pytorch: An imperative style, high-performance deep learning library. In *NeurIPS*, 2019. [5](#), [3](#)
- [61] Jonathan Ho and Tim Salimans. Classifier-free diffusion guidance. *arXiv preprint arXiv:2207.12598*, 2022. [1](#)
- [62] Kaiming He, Xiangyu Zhang, Shaoqing Ren, and Jian Sun. Deep residual learning for image recognition. In *CVPR*, pages 770–778, 2016. [1](#)
- [63] Diederik P Kingma and Jimmy Ba. Adam: A method for stochastic optimization. *arXiv preprint arXiv:1412.6980*, 2014. [3](#)

Editing 3D Scenes via Text Prompts without Retraining

Supplementary Material

6. Background of neural radiance fields and diffusion models

Neural radiance fields. NeRF utilizes an implicit function to represent scenes, which maps the spatial point $\mathbf{x} = (x, y, z)$ and view direction $\mathbf{d} = (\theta, \phi)$ to the density σ and color \mathbf{c} . Typically, the implicit function is represented by an MLP network, denoted as $F_{\Theta} : (\mathbf{x}, \mathbf{d}) \rightarrow (\sigma, \mathbf{c})$, where Θ represents the weights of the network. For a ray \mathbf{r} originating at \mathbf{o} with direction \mathbf{d} , the RGB value $\hat{\mathbf{C}}(\mathbf{r})$ of the ray is estimated through numerical quadrature of the color \mathbf{c} and density σ of the N spatial points.

$$\hat{\mathbf{C}}(\mathbf{r}) = \sum_i^N T_i (1 - \exp(-\sigma_i \delta_i)) \mathbf{c}_i, \quad (10)$$

where δ_i denotes the distance between adjacent sample points, and $T_i = \exp(-\sum_{j=1}^{i-1} \sigma_j \delta_j)$.

Text-guided diffusion models. Text-guided diffusion models aim to generate an output image z_0 from a random noise vector z_t under a textual condition \mathcal{P} . To achieve sequential denoising, the model ε_{θ} is trained to predict artificial noise, minimizing the objective:

$$\min_{\theta} E_{z_0, \varepsilon \sim N(0, I), t \sim \text{Uniform}(1, T)} \|\varepsilon - \varepsilon_{\theta}(z_t, t, \mathcal{C})\|_2^2, \quad (11)$$

where \mathcal{C} denotes the embedding of the text condition, and z_t is a noised sample according to the timestamp t . When inference, given a vector z_T , its noise is gradually removed by sequential prediction using a trained network for T steps [39]. Amplifying the effect induced by the conditioned text is a significant challenge in a text-guided generation. To address this issue, Ho et al. [61] propose a guidance technique that eliminates the need for a classifier in unconditional prediction and extends it to conditioned prediction scenarios. With the introduced concept of a null text embedding, denoted as \emptyset , and a guidance scale parameter w , then the guidance prediction is given by:

$$\tilde{\varepsilon}_{\theta}(z_t, t, \mathcal{C}, \emptyset) = w \cdot \varepsilon_{\theta}(z_t, t, \mathcal{C}) + (1-w) \cdot \varepsilon_{\theta}(z_t, t, \emptyset). \quad (12)$$

In our experiments, we primarily control the degree of image editing by adjusting the parameters w and T .

7. Network architecture

Initially, we utilize a UNet-like network with the ResNet34 [62] backbone to extract features from both the unedited and edited source views. These feature maps are

then concatenated and inputted into subsequent CNN networks to derive the final feature maps. When estimating the color \mathbf{c} and density σ of sampled points along the rays, we primarily employ the MLP networks to integrate information from the edited images, feature maps, and viewing directions. For density prediction, we adopt a design of transformer networks inspired by IBRNet [6]. Regarding the color estimation, we incorporate additional pixel difference information among source views to capture the extent of editing across different perspectives, aiding the network in improved learning. The detailed network architecture and data propagation process are depicted in Figure 16.

8. Additional implementation details

8.1. Generating training data pairs

Generate input and target captions. During the training phase, we utilized a total of 1246 scenes. For each scene, we randomly select one image to generate an input caption using the BLIP model [31] with 2.7 billion parameters¹. A subset of the generated captions is shown in Figure 10. Then we utilize the GPT model [32] to generate target captions. As shown in Table 4, the four instruction prompts for GPT are:

- (1). List 100 famous painters.
- (2). List 50 famous painting schools.
- (3). List 100 famous paintings.
- (4). Replace, add, or delete partial words in the following sentences: X. (X is the input caption from BLIP.)

During training, we select one of the above (1)-(4) following a 2:2:2:4 ratio to generate the target caption. For (1), a chosen painter like ‘‘Van Gogh’’ could transform the caption ‘‘a red flower’’ into ‘‘Van Gogh painting of a red flower’’. Similar procedures apply to (2) and (3). For (4), GPT might change ‘‘a red flower’’ to ‘‘a red apple’’. Thus, each scene incorporates 405 target captions.

Minor perturbations for training. We generate the training data by applying minor random perturbations to the 3D scene using the Null-text². The relevant parameters are set as follows: 100 to 300 for the iteration number T and 0.5 to 3.5 for the text guidance scale w .

Normal perturbations for inference. For normal-scale edits, we follow the recommended settings from the Null-text paper, with $w=7.5$ and $T=500$.

The effects of applying random minor perturbations and normal editing to the images are depicted in Figure 11.

¹<https://huggingface.co/Salesforce/blip2-opt-2.7b>

²<https://null-text-inversion.github.io>



Figure 10. **Generate input captions by BLIP.** We randomly select an image in a 3D scene to generate its input caption by BLIP [31].

Table 4. **Generate target captions by GPT.** Given the input caption S for a 3D scene, we utilize GPT [32] to generate a target caption O . For instance, if S is 'yellow roses in the garden', the target captions can be 'Leonardo da Vinci painting of yellow roses in the garden', 'yellow roses in the garden in the Rococo style', 'pink roses in the garden', to name a few.

Prompts	List 100 famous painters	List 50 famous painting schools	List 100 famous paintings	Replace, add or delete partial words in the following sentences: S_1, S_2, \dots
GPT outputs (O)	Leonardo da Vinci Vincent van Gogh Pablo Picasso ⋮ ⋮	Baroque Realism Impressionism ⋮ ⋮	Mona Lisa The Last Supper The Scream ⋮ ⋮	pink roses in the garden red roses in the garden white roses in the garden ⋮ ⋮
	Henri Matisse Eva Hesse Carl Andre	Tonalism Ashcan School Rococo	The Fifer The Kiss The Hay Wagon	a green couch with gold trim a green chair with silver trim a green chair with no trim
Target captions	O painting of S or S in the O style	O painting of S or S in the O style	S in the O style	O

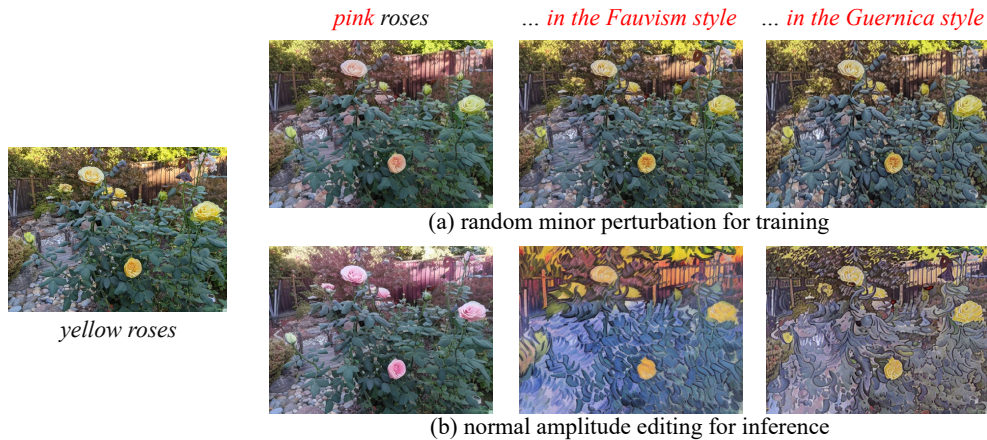


Figure 11. **Visualization of random minor perturbations and normal amplitude editing.** The proposed model learns to remove the added perturbations on (a). Upon completion of the learning process, the model generates consistent editing results by eliminating inconsistencies between images subjected to normal amplitude editing on (b).

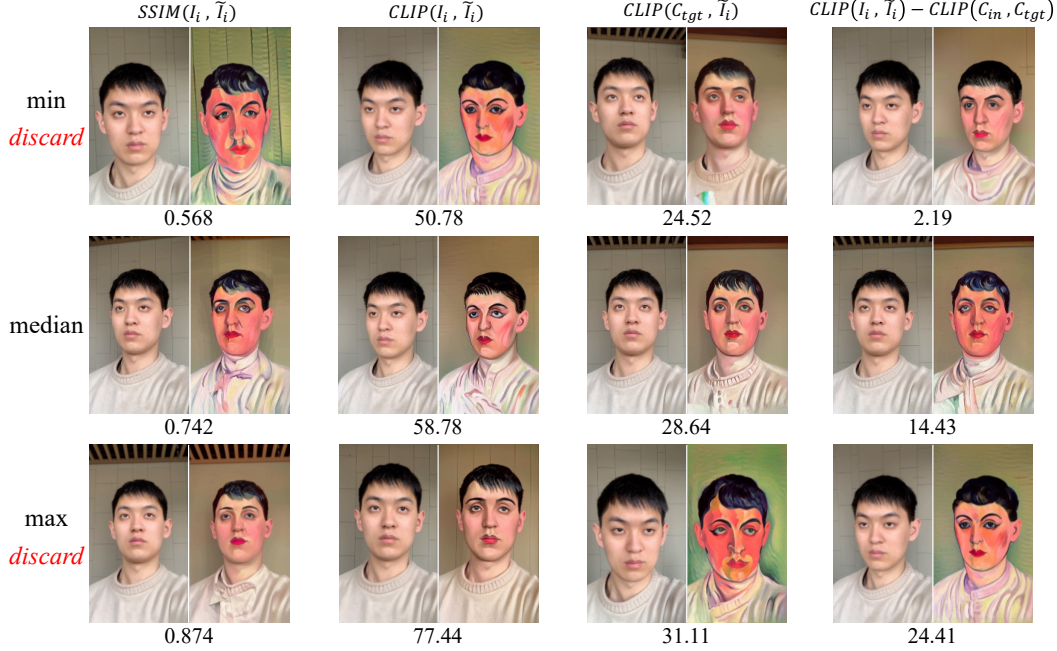


Figure 12. Visualize the editing results of the 2D editing model, as well as the maximum, minimum, and median values for each metric of the content filter. The images that correspond to the minimum and maximum values often exhibit either low or excessive editing degrees. By discarding them, we can enhance the 3D consistency among the remaining images.

8.2. Details of training and inference

Training phase. Our method is implemented using the PyTorch framework [60]. We employ the Adam optimizer [63] with initial learning rates of $1e-4$ for the CNN and $5e-4$ for the MLP. The training process runs for 300K steps with a batch size of 500 rays. The initial values for the loss weight in Eq. 8 in the main text of l_{self} , l_{nbr} , l_{en} , and l_{tv} , are set as $\lambda_1=1e-3$, $\lambda_2=1e-3$, $\lambda_3=1e-3$, and $\lambda_4=2e-3$, respectively. The calculation of l_{nbr} is only performed after the iteration count exceeds 10K. During the training phase, we randomly select a variable number of source views ranging from 6 to 15, while using 15 source views during inference. The number of sampled points on a ray is set to 64.

Inference phase. After completing the training process, given a scene and its corresponding textual description, we apply normal-level editing to the images of the scene. Following that, we employ a content filter to select the edited results, removing the lowest and highest 10% of values for each of the four metrics defined in Eq. 9 in the main text.

Implementation details of the content filter. The main idea behind the content filter is to maintain the degree of editing consistent across various perspectives. To achieve this, we consider the following two situations:

(1). A smaller degree of editing implies fewer changes in the *edited image* relative to the *original image* and *input caption*, while a larger discrepancy with the *target text*.

(2). Conversely, a higher degree of editing denotes more significant changes in the *edited image* compared to the *original*, bringing it closer to the *target text*.

Therefore, the evaluation metrics used in the content filter can be measured through the relationship between the original image, edited image, original text description, and target text description. Specifically, given an original image I_i and its caption C_{in} , as well as its corresponding edited image \tilde{I}_i and its caption C_{tgt} , we calculate the following four measurements based on SSIM similarity and CLIP similarity during the filtering process:

- (a). $SSIM(I_i, \tilde{I}_i)$
- (b). $CLIP(I_i, \tilde{I}_i)$
- (c). $CLIP(\tilde{I}_i, C_{tgt})$
- (d). $CLIP(I_i, \tilde{I}_i) - CLIP(C_{in}, C_{tgt})$

Here, the metrics (a) and (b) assess the similarity between the image before and after editing. The metric (c) gauges the similarity between the edited image and the target caption, while the metric (d) evaluates the relative offset between the text and the image. These indicators assess the editing results on different dimensions. The role of our content filter is to eliminate extreme values (top 10% and bottom 10%) from these metrics, ensuring metric values between the remaining images are not significantly different.

In Figure 12, we provide the maximum, minimum, and median values for each of the aforementioned metrics, along with their corresponding original and edited images.

Table 5. **Quantitative comparison of CLIP Directional Score (CDS) and CLIP Consistency Score (CCS)**. CDS* indicates using a different caption from CDS. CCS* means our result at the minimum editing degree. *The displayed values are multiplied by 100.*

	Van Gogh				Fauvism			
	CDS	CDS*	CCS	CCS*	CDS	CDS*	CCS	CCS*
NeRF-Art	13.07	10.21	2.06	2.06	17.38	12.74	1.38	1.38
Instruct-N2N	11.21	10.39	9.24	9.24	16.62	13.18	4.11	4.11
Ours	8.83	11.76	4.89	100	14.06	14.93	2.29	100

Figure 12 shows that the editing results with maximal and minimal metric values exhibit larger image discrepancies. These will pose greater challenges for subsequent 3D consistency. Our content filter, by eliminating these extreme editing results, facilitates superior 3D editing outcomes.

9. Additional quantitative comparison

Although the evaluation of the editing results is subjective, we follow the descriptions of CLIP Directional score (CDS) and CLIP Consistency score (CCS) as outlined by Instruct-N2N [23] to quantitatively evaluate the editing results shown in Figure 3 of the main text. The quantitative results are presented in Table 5. It is clear that, under different settings, there are large variances in these metrics.

The CDS measures how much the change in text captions agrees with the change in images. When using CDS, different descriptions yield varying results, as shown by CDS and CDS* in Table 5. This is mainly because the prompts used in training vary across different methods. For example, NeRF-Art just uses target words like “Van Gogh”, and incorporates the CDS into the loss function (as in Equation 4 of the NeRF-Art paper), while Instruct-N2N employs instructional prompts such as “Make him look like Vincent Van Gogh”. Our method, on the other hand, provides a target description like “Vincent Van Gogh is in front of the wall.” Thus, providing an equitable text description for comparing CDS presents a challenge. With the description “Portrait of Van Gogh”, NeRF-Art has a higher CDS. When “Vincent Van Gogh is in front of the wall” is provided, our method performs the best. Therefore, CDS may not fully evaluate image editing performance effectively.

The CCS measures the cosine similarity of the CLIP embedding of each pair of adjacent frames in a novel camera path. This metric heavily depends on the degree of editing. In extreme cases where the edited result is identical to the unedited one, the CCS has a max value (close to 1). However, under such conditions, the editing effect is not achieved. Therefore, the CCS also has certain limitations.

Due to these considerations, both DN2N and Instruct-N2N mainly compare with other methods for visual effects, rather than for CDS and CCS metrics. Effective quantitative comparison for editing results remains challenging, so existing methods still opt for subjective evaluations, for in-

stance, by conducting user studies to aggregate subjective evaluation results from multiple individuals in order to reflect the quality of the editing results.

10. Additional ablation studies

In this section, we present additional ablation experiments related to the training data generation, content filter, self-view (l_{self}), and neighboring-view (l_{nbr}) regularization terms. Specifically, we edit the flower scene in the LLFF dataset to a transparent ice sculpture flower. The ablation results are shown in Figure 13 and Figure 14

Without perturbed data generation, we observed significant color and gloss discontinuities between different novel views in the editing results as shown in Figure 13. This is mainly due to the model not learning how to remove inconsistent perturbations between images. In the inference stage, the normal editing may cause substantial consistency disruption in 2D editing results, this is mitigated by the content filter. Removing this filtering process leads to noticeable inconsistencies in the results as depicted in Figure 13. The situation in Figure 14 is similar, noticeable inconsistencies in color or brightness can be seen when removing the l_{self} and l_{nbr} regularization terms.

11. User study details

We invited a total of 50 subjects (31 males and 19 females) to participate in the user study. Each participant is presented with videos or frames generated by various methods. They are asked to select their preferred option based on three distinct criteria. An example of the questionnaire is available in Figure 15. Typical questions in the questionnaire are:

- (1). What is the video with higher consistency?
- (2). Please select an image that retains more of the original image content.
- (3). Please select an image that more closely matches the text description.

We use 23 videos to evaluate 3D consistency, and 24 images to measure content preservation and faithfulness to the text description. After completing the survey, we tally user support rates for our method compared to other methods, as shown in Figure 7 in the main text.

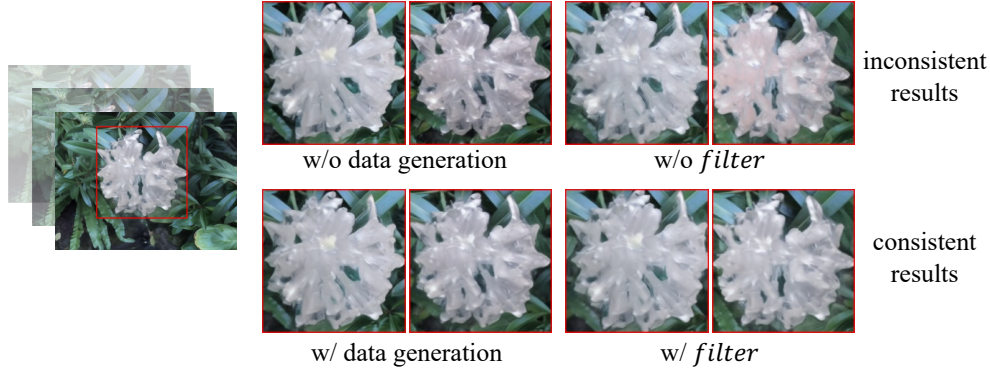


Figure 13. **Ablation study on data generation and content filter.** Without incorporating data augmentation involving minor perturbations and the content filter component, the rendered novel views may exhibit noticeable inconsistencies in terms of glossiness and color.

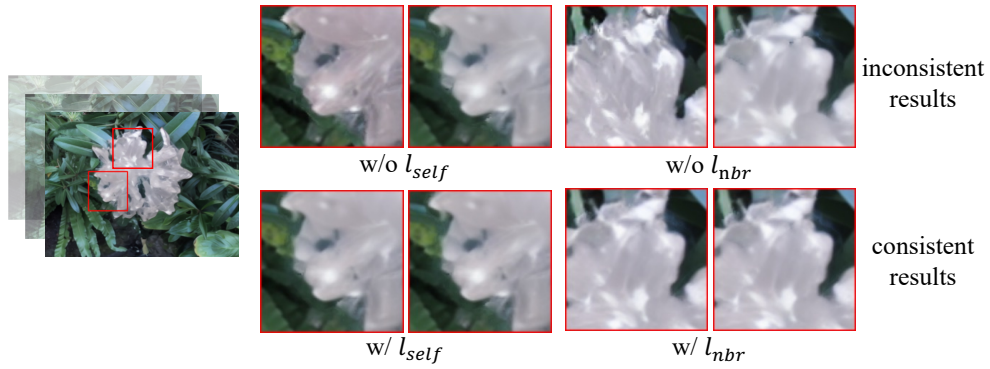


Figure 14. **Ablation study on l_{self} and l_{nbr} regularization terms.** Without the l_{self} , the 3D consistency of the rendering results under different source views is poor. And without the l_{nbr} , inconsistency exists among different neighboring views.

Please select an image that meets the following criteria:
 1. Retained more of the original image content;
 2. More closely matched with the text 'white flower';

			
Content retention	<input type="radio"/>	<input type="radio"/>	<input type="radio"/>
text matching degree	<input type="radio"/>	<input type="radio"/>	<input type="radio"/>

What is the video with higher “3D-consistency” ?

			
consistency	<input type="radio"/>	<input type="radio"/>	<input type="radio"/>

Figure 15. **Example of questionnaire for user study.**

12. Visualization of geometric information

We visualize the depth maps before and after scene editing, as shown in Figure 17. This is divided into two cases: first, when only appearance is edited, the depth maps before and after exhibit negligible differences. Second, for edits altering the geometry of objects, the depth maps correspondingly exhibit changes as well, validating the 3D awareness of our editing approach.

13. Additional editing results

In this section, we present a collection of additional editing results that showcase the remarkable editing capabilities and effects of our method. The results are shown as Figure 18 Figure 19, Figure 20, and in Figure 21.

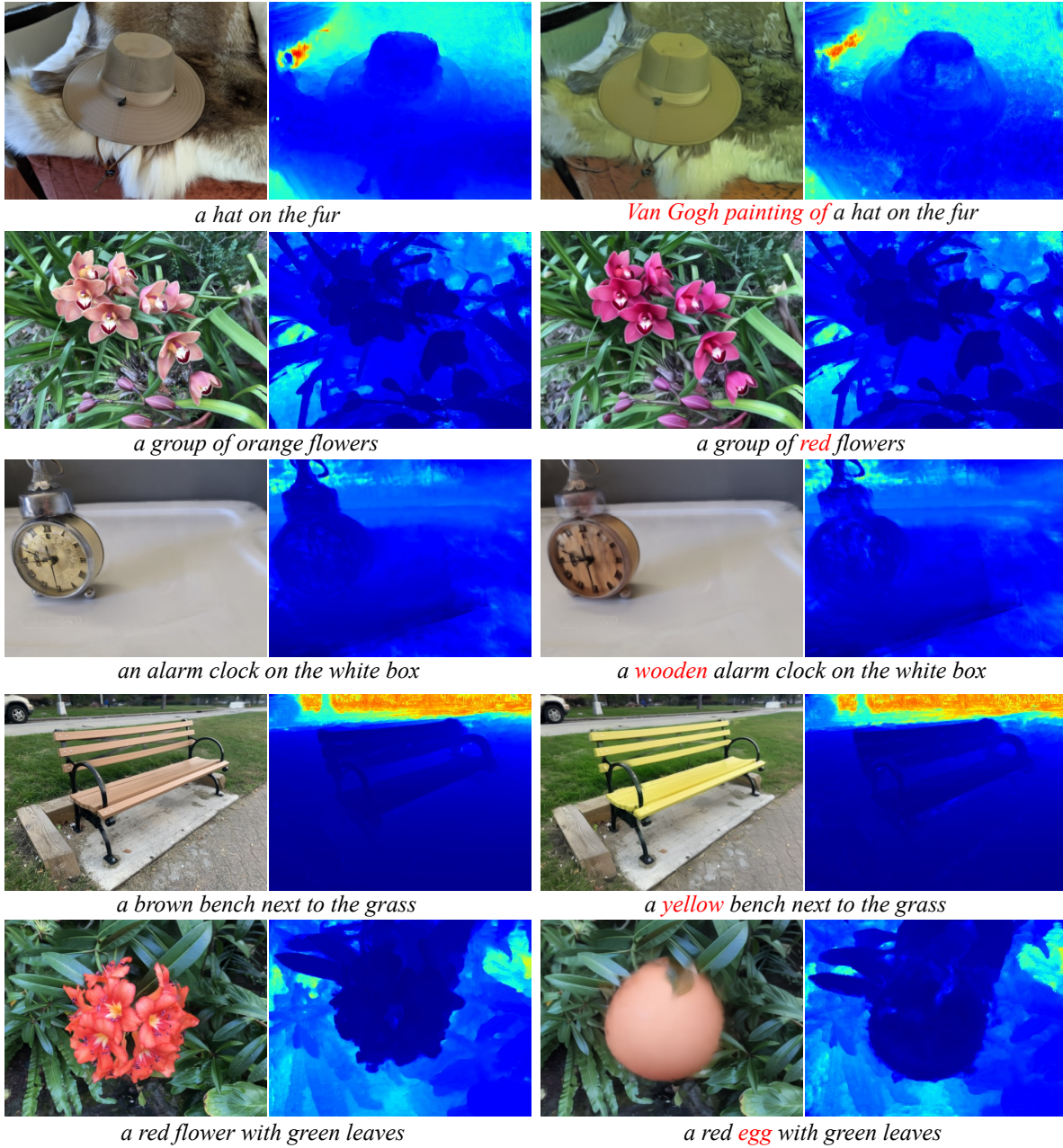
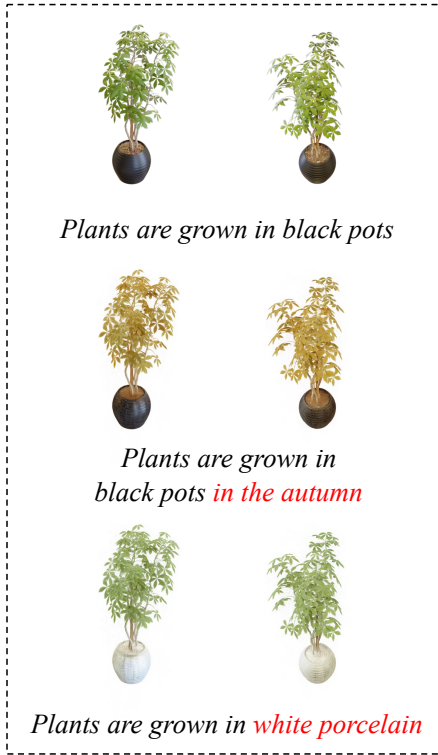


Figure 17. Visualization of geometric information.



(a) NeRF-Synthetic dataset

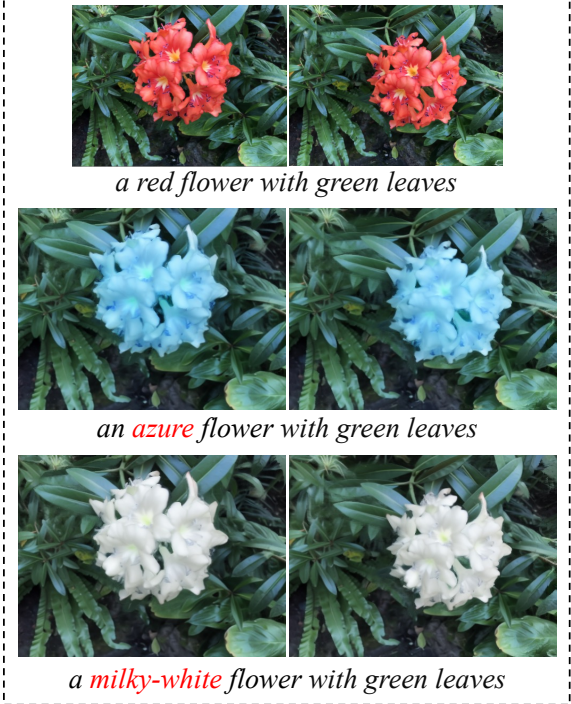


(b) OMMO dataset

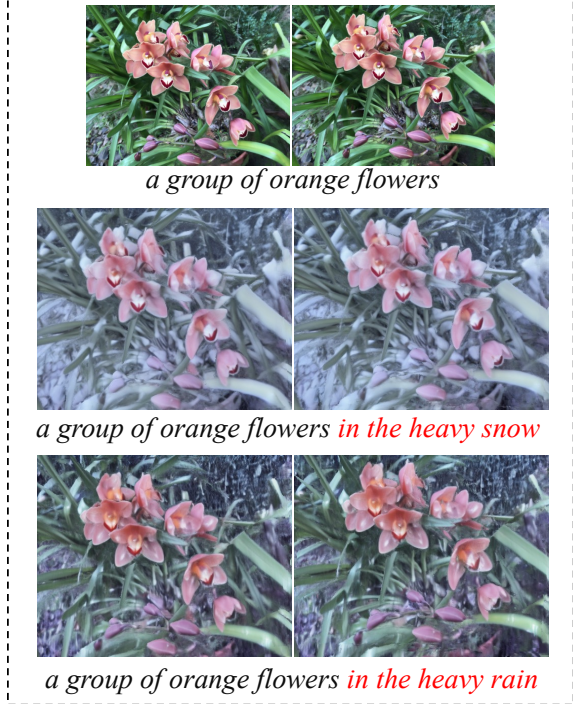


(c) KITTI dataset

Figure 18. More visual results on NeRF-Synthetic, OMMO, and KITTI datasets. The NeRF-Synthetic dataset [1] is synthetic scenes. The OMMO dataset [58] is 360° scenes captured by the drone camera. The KITTI dataset [59] is the street view scenes captured by the car camera.



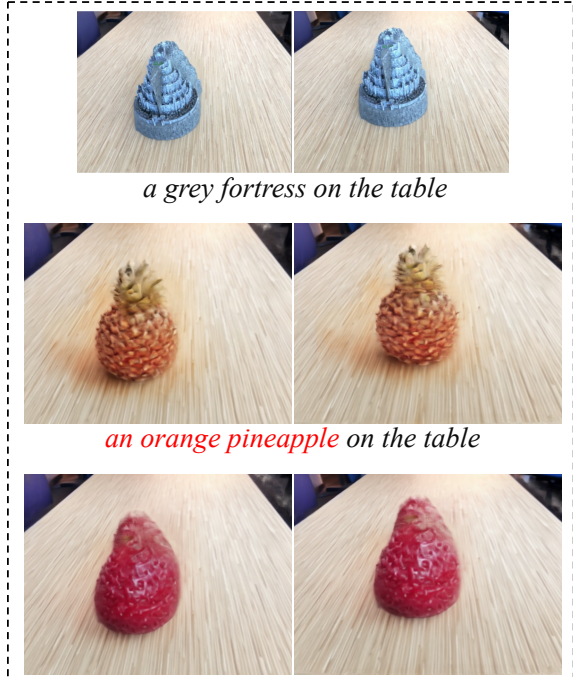
(a) appearance editing



(b) weather transformation



(c) style transfer



(d) object changing

Figure 19. More visual results on LLFF dataset.



a man is in front of the wall



a golden man sculpture is in front of the wall



a wood man sculpture is in front of the wall



a silver man sculpture is in front of the wall



a man with yellow hair is in front of the wall



a woman is in front of the wall



a child is in front of the wall



an old man is in front of the wall



a saiyan is in front of the wall



a man with closed eyes is in front of the wall



a man with glasses is in front of the wall



a man with suit is in front of the wall



The Tolkien Elf is in front of the wall

Figure 20. More visual results on portrait editing.

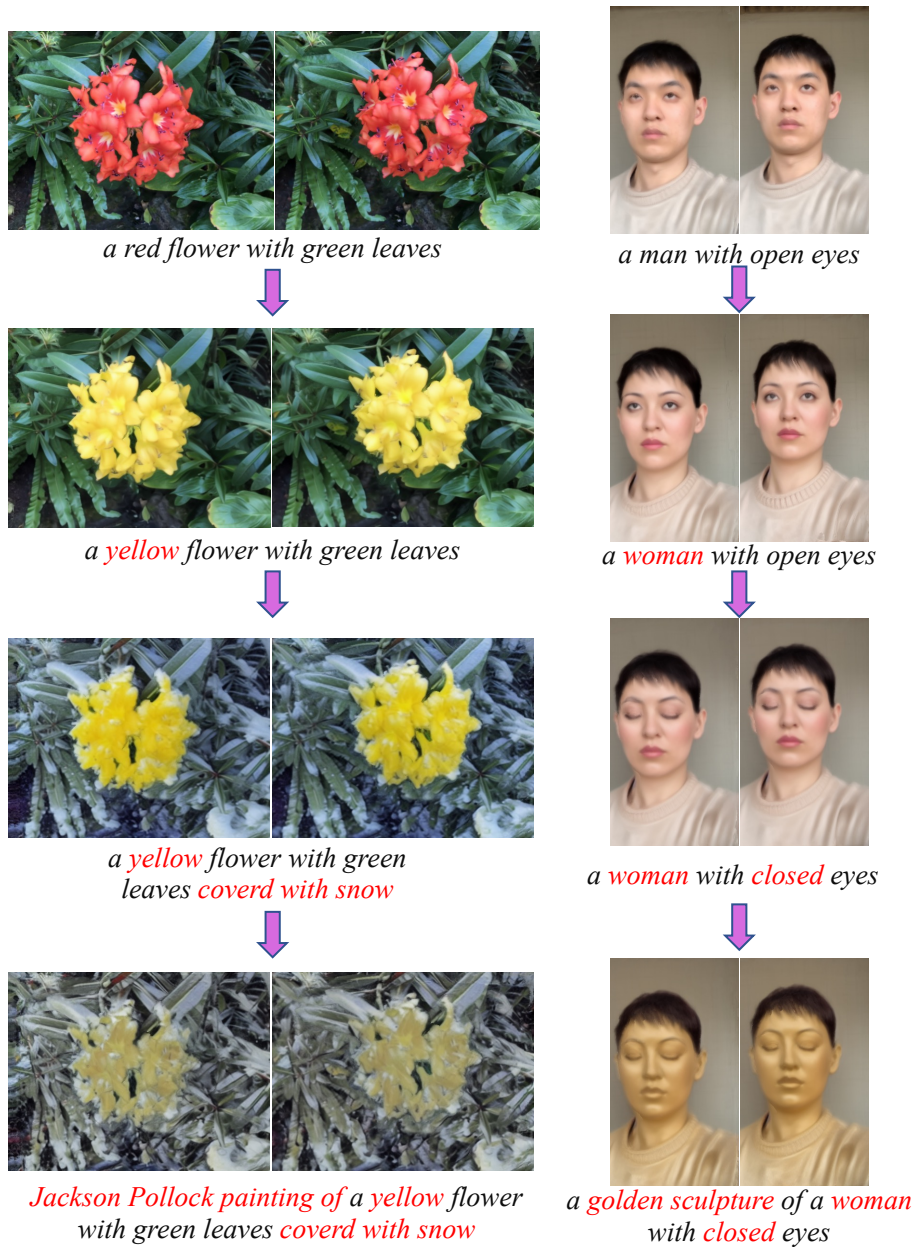


Figure 21. **Cascade editing results.** We begin by applying an edit to the original scene and then generate a new scene with the desired editing effect using DN2N. We repeat this process by applying another edit to the new scene. In this figure, we showcase the consecutive results of three cascaded edits.